

Ultrahigh-energy Gamma Rays and Gravitational Waves from Primordial Exotic Stellar Bubbles

Yi-Fu Cai,^{1,2,3,*} Chao Chen,^{1,2,3,†} Qianhang Ding,^{4,5,‡} and Yi Wang^{4,5,§}

¹*Department of Astronomy, School of Physical Sciences,*

University of Science and Technology of China, Hefei, Anhui 230026, China

²*School of Astronomy and Space Science, University of Science and Technology of China, Hefei, Anhui 230026, China*

³*CAS Key Laboratory for Research in Galaxies and Cosmology,*

University of Science and Technology of China, Hefei, Anhui 230026, China

⁴*Department of Physics, The Hong Kong University of Science and Technology,*

Clear Water Bay, Kowloon, Hong Kong, P.R.China

⁵*Jockey Club Institute for Advanced Study, The Hong Kong University of Science and Technology,*

Clear Water Bay, Kowloon, Hong Kong, P.R.China

We put forward a novel class of exotic celestial objects that can be produced through phase transitions occurred in the primordial Universe. These objects appear as bubbles of stellar sizes and can be dominated by primordial black holes (PBHs). We report that, due to the processes of Hawking radiation and binary evolution of PBHs inside these stellar bubbles, both electromagnetic and gravitational radiations can be emitted that are featured on the gamma-ray spectra and stochastic gravitational waves (GWs). Our results reveal that, depending on the mass distribution, the exotic stellar bubbles consisting of PBHs provide not only a decent fit for the ultrahigh-energy gamma-ray spectrum reported by the recent LHAASO experiment, but also predict GW signals that are expected to be tested by the forthcoming GW surveys.

Introduction – With dramatic developments of observational technologies, a large number of new phenomena have been discovered in various astronomical experiments in the past decade. Our understanding of the very nature of Universe, especially of the exotic astrophysical objects including black holes, supernovae, neutrons, blazars, dark matter (DM) and active galactic nuclei, has been greatly developed. Specifically, the high-energy gamma-ray observations provide the only available probe to identify cosmic-ray sources which could tell us the unique information about the exotic celestial objects, as gamma rays travel straightly from the source without the deflection by galactic magnetic field [1, 2]. However, many of cosmic-ray sources have physical origins that are still under discussion [3, 4].

Also, accumulated gravitational wave (GW) events detected by the LIGO/Virgo Collaboration started a new era in the observational astronomy, that shed light on the formation of exotic astrophysical objects [5], and have been used to test general relativity in the unexplored strong gravity regime [6]. Hence, the development of the multi-messenger observation, which is a joint observation of cosmic rays, neutrinos, photons and GWs, could provide us the unique insights into the properties of astrophysical sources and source populations in our Universe [7]. With the multi-messenger observation, there is a growing interest in searching for exotic celestial bodies, such as quark stars [8], boson stars [9], dark stars [10] and antistar [11], etc. Their search can reveal new aspects of fundamental science and serve as new probes into the primordial Universe.

In this Letter, we propose a novel class of exotic celestial objects filled by primordial black holes (PBHs).

These objects appear as bubbles of stellar sizes and can emit gamma rays and GWs through the processes of Hawking radiation and binary mergers, respectively. Theoretically, these stellar bubbles can be generated from some new-physics phenomena that might have occurred in the primordial Universe, such as, quantum tunnelings during or after inflation [12, 13], multi-stream inflation [14], inhomogeneous baryogenesis [15], etc. In these cases, before the bubble-wall tension vanishes, the field values are different between inside and outside of the bubble. Such difference can result in different local physics inside the bubble, namely the production rate of the exotic species of matter illustrated below, which indicates the existence of the “*island universes*”, as a baby version of a *multiverse*. If the sizes of these bubbles are small enough, say, smaller than the resolution of current telescopes, they behave as exotic celestial objects.

Observational consequence of exotic stellar bubbles can arise from: (i) Decay, annihilation or interaction of exotic matter inside the bubble, for example, unstable particles, textures, monopoles, cosmic strings, domain walls, and PBHs, etc, that can yield cosmic rays at high energy scales and hence may address the puzzle of ultrahigh-energy cosmic rays, such as PeV gamma rays discovered in the recent LHAASO observation [16]; (ii) Interaction at the interface of the bubble, for example, if the stellar bubble is made of antimatter, where the effects can be in analogy to [11]. If there are overdense regions inside the bubble, certain amount of PBHs can be formed due to the local gravitational collapse [17–19], resulting in a wide range of PBH masses which is quite different from the astrophysical black holes [20–22]. When these PBHs’ masses are small enough, their Hawking radiations

become significant to generate observable electromagnetic (EM) signals. Additionally, PBHs can also cluster to form binaries and generate GWs from their mergers [23, 24]. As such, it is expected to search for the nontrivial observational signals from these exotic celestial bodies, as we will investigate in this Letter.

EM radiations – In [25, 26] Hawking found remarkably that black holes emit radiations in the black-body form. This mechanism can be applied into PBHs that were formed in the very early Universe [27]. Theoretically, the PBHs satisfy a certain mass distribution depending on the underlying generation mechanisms [28–31], and hence one can derive the EM radiations contributed by all possible mass scales. Let us focus our interest on neutral PBHs of the Schwarzschild type. The time-dependent physical number density n_i of elementary particle i emitted by a distribution of PBHs per unit time and per unit energy can be determined by

$$\frac{d^2 n_i}{dt dE}(E) = \int_{M_{\min}}^{M_{\max}} \frac{d^2 N_i}{dt dE}(E, M) n_{\text{PBH}}(M) dM, \quad (1)$$

where $d^2 N_i/dt dE$ is the Hawking instantaneous emission rate for particle i . The lower mass limit M_{\min} is usually set to the Planck mass $M_{\text{pl}} \simeq 2 \times 10^{-5}$ g, while the upper one M_{\max} can be infinity.

In general, the mass distribution of PBHs can be described by the differential physical mass function $n_{\text{PBH}}(M) \equiv dn_{\text{PBH}}/dM$, where dn_{PBH} is the physical number density of PBHs in the mass range $(M, M + dM)$. For heavy PBHs which survive at present (the formation mass $M_f \gtrsim 10^{15}$ g), the current energy fraction f_{PBH} of PBHs over the DM component is given by the integral $f_{\text{PBH}} \equiv \Omega_{\text{PBH}}/\Omega_{\text{DM}} = \int_{M_{\min}}^{M_{\max}} \psi(M) dM$, where Ω_{PBH} and Ω_{DM} are the current normalized density of PBHs and DM, respectively. The current mass function $\psi(M)$ is defined as $\psi(M) \equiv M n_{\text{PBH}}(M)/\rho_{\text{DM}}$, where the scale factor at present takes $a(t_0) = 1$. If the PBHs were from inflationary fluctuations, they naturally satisfy a lognormal mass function [22, 32],

$$\psi_{\text{LN}}(M) = \frac{f_{\text{PBH}}}{\sqrt{2\pi}\sigma M} \exp\left[-\frac{\ln^2(M/M_{\text{pk}})}{2\sigma^2}\right], \quad (2)$$

where the subscript ‘‘LN’’ denotes the lognormal type. Given f_{PBH} , there are two parameters in $\psi_{\text{LN}}(M)$: σ describes the width of mass distribution and M_{pk} is the mass at which the function $M\psi_{\text{LN}}(M)$ (the DM fraction in PBHs at the logarithmic interval around M) peaks. Since light PBHs ($M_f \lesssim 10^{15}$ g) would have evaporated at earlier time, the present mass function could be deformed from the initial shape, especially in the low-mass tail [33].

The extragalactic gamma-ray background (EGB) is an important constraint for evaporating PBHs [34]. With the advent of gamma-ray experiments in various energy ranges, such as the Imaging Compton Telescope (COMPTEL) for 0.8 ~ 30 MeV [35], the Energetic Gamma Ray

Experiment Telescope (EGRET) for 20 MeV ~ 30 GeV [36], the Fermi Large Area Telescope (Fermi LAT) for 20 MeV ~ 300 GeV [37], PBHs within the mass range $10^{14} \sim 10^{16}$ g are severely constrained and cannot provide the dominant contribution to DM [27, 38, 39]. Moreover, the galactic gamma-ray background [33] and gamma-ray bursts [40, 41] can be applied to constrain PBHs.

Now, we study the EM signals from a single PBH stellar bubble and the possibility of their detection by high-energy gamma-ray experiments. We mention that multiple bubbles can be considered as independent single bubble events for observations. Consider a PBH stellar bubble located at redshift z , with an initial lognormal mass distribution (2). The key EM observable is the photon flux detected on Earth $F(\tilde{E}, t) \equiv \tilde{E}^2 d^2 \tilde{n}_\gamma / d\tilde{E} dt$, where \tilde{E} and \tilde{n}_γ are the photon energy and number density observed on Earth. This observed photon flux is related to the intrinsic luminosity $L(E, z)$ of Hawking radiation from the PBH bubble located at z via

$$F(E, z) = \frac{L(E, z)}{4\pi d_L^2(z)}, \quad (3)$$

where $L(E, z)$ is determined by the emitted photon physical number density per unit energy and per unit time $d^2 n_\gamma / dt dE$. It can be numerically computed as shown in the upper left panel of Fig. 1 for the peak masses $M_{\text{pk}} = 10^{13}, 10^{15}, 10^{17}$ g and the energies of emitted photons $E = 10, 100$ GeV, respectively. The flat parts in this panel are caused by small masses radiating at the early stage of Hawking radiation. The luminosity distance in Eq. (3) is given by $d_L(z) = (1+z) \int_0^z d\tilde{z}/H(\tilde{z})$, which accounts for the redshift of the photon energy and apparent emission rate [42, 43]. Combing (1) and (3) yields the observed photon fluxes in various photon energy ranges from a single PBH bubble located at z , as reported in the upper right panel of Fig. 1. It shows that for the small peak mass $M_{\text{pk}} = 10^{13}$ g, the observable fluxes of the PBH bubble of redshift $z \gtrsim 1$ would increase to some extent in contrast to the larger peak mass $M_{\text{pk}} = 10^{15}, 10^{17}$ g. This is because that a majority of PBH bubbles with small M_{pk} could evaporate at high redshifts.

Gamma-ray signals – Recall that the PBH mass function in (2) relies on three parameters, i.e., f_{PBH} , σ and M_{pk} . Even in the case that the PBHs disappeared at the early time, one can generalize the concept of f_{PBH} to be the total PBH density at a certain time against the present DM density, which is consistent with the standard definition of f_{PBH} , and convenient for our calculation. Furthermore, the intrinsic luminosity of Hawking radiation involves two other parameters of a bubble, i.e., its physical volume V and redshift z . Note that, one can combine f_{PBH} and V to yield the initial total mass of a PBH bubble M_{bub} which is of observable interest (It is reasonable to assume that the total mass of the bubble is dominated by PBHs for detectable signals, as we will show below). Thus, we get four parameters: M_{bub} , z ,

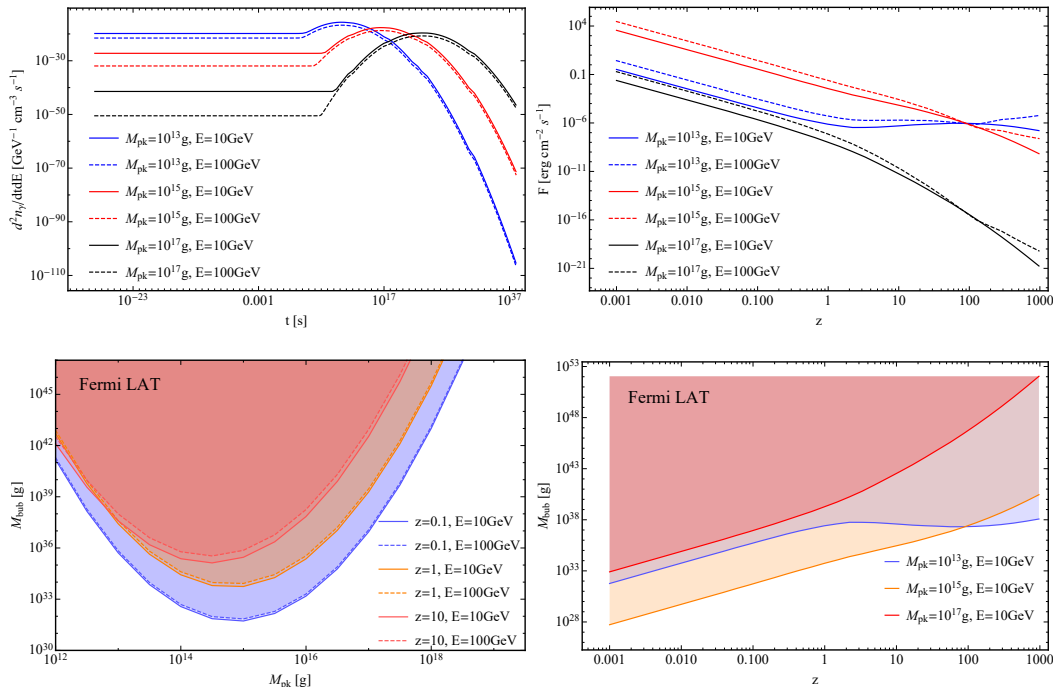


FIG. 1. *Upper left:* The spectrum $d^2 n_\gamma / dt dE$ of a PBH bubble as a function of cosmic time t for peak masses $M_{\text{pk}} = 10^{13}, 10^{15}, 10^{17}\text{g}$ and photon energies $E = 10, 100\text{GeV}$, respectively. For simplicity, we have set $f_{\text{PBH}} = 1$ and $\sigma = 1$. *Upper right:* The observed photon flux F of a PBH bubble of physical volume 1Mpc^3 located at different redshifts, for various peak masses and photon energies. *Lower left:* The parameter space of the peak mass M_{pk} and bubble mass M_{bub} of a PBH bubble allowed by Fermi LAT (the shaded regions) for redshifts $z = 0.1, 1, 10$ and photon energies $E = 10, 100\text{GeV}$, respectively. *Lower right:* The parameter space of the redshift z and bubble mass M_{bub} allowed by Fermi LAT (the shaded regions) with the photon energy $E = 10\text{GeV}$ and peak masses $M_{\text{pk}} = 10^{13}, 10^{15}, 10^{17}\text{g}$, respectively.

M_{pk} and σ . Using the point-source differential sensitivity in the 10-year observation of Fermi LAT for a high Galactic latitude (around the north Celestial pole) source [37], we numerically derive the experimentally allowed parameter spaces for $(M_{\text{bub}}, M_{\text{pk}})$ and (M_{bub}, z) by the shaded regions in the lower panels of Fig. 1, respectively. Setting $\sigma = 1$, for given redshifts and photon energies, the lower bound of the parameter space for M_{pk} and M_{bub} is around $M_{\text{pk}} \simeq 10^{15}\text{g}$, which is the mass scale evaporating at present, and the corresponding bubble mass is $M_{\text{bub}} \simeq 10^{32}\text{g} \sim M_\odot$, close to one solar mass. For the smaller or larger values of M_{pk} , the corresponding Hawking radiation has either decayed out already or not yet become efficient, and thus the bubble mass M_{bub} needs to be heavy enough to yield observable evidences. Additionally, two lower panels of Fig. 1 indicate that, the closer the stellar PBH bubbles are to the Earth, the easier they could be probed. The ‘‘plateau’’ for the case of $M_{\text{pk}} = 10^{13}\text{g}$ and $z \gtrsim 1$ appeared in the lower right panel of Fig. 1 is due to the same reason for the fluxes of $M_{\text{pk}} = 10^{13}\text{g}$ shown in the upper right panel.

Recently, the LHAASO experiment reported the astonishing detection of twelve ultrahigh-energy gamma-ray sources [16], which indicates some high energy physics in stellar objects. While the astrophysical sources responsi-

ble for these events are under debate [1, 2, 44], it deserves to examine the possibility of their origins being exotic celestial objects including the PBH stellar bubble. Therefore, we confront our scenario with the latest LHAASO data and report the numerical results in the left panel of Fig. 2. In order to examine the relation between the gamma-ray spectrum and the present PBH mass distribution, the present lognormal distribution is considered instead of a primordial one. Accordingly, \tilde{M}_{pk} denotes the peak mass of present lognormal distribution, and \tilde{M}_{bub} denotes the present stellar bubble mass. In the numerical calculations, we set $\sigma = 1$. Allowing σ to vary may lead to better fits to observations, which we will not explore in the present work. Our results illustrate well that the PBH stellar bubbles can provide a decent fit as shown in the plot explicitly.

GW signals – The PBH formation and the evolution of PBH binaries produce GWs. It is known that PBHs are formed with mass $M_{\text{PBH}} \sim c^3 t / G$, and thus if they were formed within 1 second after the big bang, the corresponding PBH mass is less than $10^4 M_\odot$ and the associated GWs become very weak for observations. Accordingly, the main observational channel of GWs is to follow the evolution of PBH binaries when considering heavy masses.

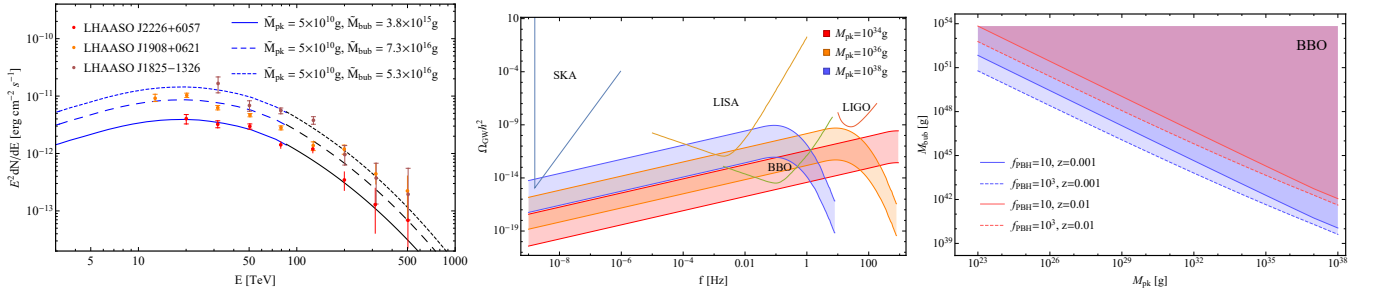


FIG. 2. *Left*: The fit of three different PBH stellar bubbles to the data by LHAASO. The observation distance of ultrahigh-energy gamma-ray sources J2226 + 6057, J1908 + 0621, J1825 - 1326 are 0.8, 2.37, 1.55 kpc [45, 46], respectively. The blue curves are numerical results produced using the publicly available code BlackHawk [47], and the black curves are the superpositions of analytic black body spectra normalized by the BlackHawk calculation. *Middle*: The GW spectrum of a PBH stellar bubble. We set $f_{\text{PBH}} = 1$ in the bubble and $z = 0.01$. The mass distribution of PBHs is lognormal with $\sigma = 1$ and $M_{\text{pk}} = 10^{34}, 10^{36}, 10^{38}$ g for red, orange, blue shadow regions respectively. The lower and upper solid curves denote the total PBH mass in a bubble, which are set as 10^{45} g and 10^{48} g, respectively. Sensitivity curves of SKA [48], LISA [49], BBO [50] and LIGO [51] are plotted. *Right*: The parameter space of the bubble mass and peak mass of a PBH bubble that can be probed by BBO at 0.1 Hz with $\Omega_{\text{GW}} h^2 = 2.9 \times 10^{-15}$. The solid and dashed lines denote $f_{\text{PBH}} = 10, 10^3$, respectively. Blue and red shaded regions denote $z = 0.001, 0.01$, respectively.

A PBH binary in a stellar bubble forms from two nearby black holes and decouples from the Hubble flow. Given the initial separation x in a binary system of total mass $M = m_1 + m_2$, the binary system decouples from the Hubble flow at $z \approx 3(1 + z_{\text{eq}})/\lambda - 1$, where $z_{\text{eq}} \approx 3000$ is the redshift at matter-radiation equality in the Λ CDM cosmology with $\Omega_M = 0.315$, $\Omega_\Lambda = 0.685$ [52], and there is $\lambda \equiv 8\pi\rho_{\text{eq}}x^3/3M$ [53].

In the binary evolution, the GW energy spectrum from a single PBH stellar bubble can be calculated by

$$\Omega_{\text{GW}}(f) = \frac{1}{\rho_c} \frac{1}{4\pi d_L^2} f_r \frac{dE_{\text{GW}}}{df_r} R, \quad (4)$$

where f is the observed GW frequency and f_r is the GW frequency in the rest frame of binaries, with $f = f_r/(1 + z)$. $\rho_c = 3H_0^2/8\pi G$ the critical density of the Universe, and R is the comoving merger rate of PBH binaries [54]. dE_{GW}/df_r is the energy emission per frequency interval, which is parameterized by [55–57]

$$\frac{dE_{\text{GW}}}{df_r} = (\pi G)^{2/3} \mathcal{M}_c^{5/3} \times \begin{cases} f_r^{-1/3} & , f_r < f_1 \\ f_r^{2/3} f_1^{-1} & , f_1 \leq f_r < f_2 \\ f_4^4 f_r^2 [f_1 f_2^{4/3} (4(f_r - f_2)^2 + f_4^2)]^{-1} & , f_2 \leq f_r < f_3 \end{cases} \quad (5)$$

where $\mathcal{M}_c \equiv (m_1 m_2)^{3/5} / M^{1/5}$ is the chirp mass of the binary system and $f_i = (a_i \eta^2 + b_i \eta + c_i) / \pi G M$. The symmetric mass ratio η is defined as $\eta \equiv m_1 m_2 / M^2$ and the coefficients a_i, b_i, c_i can be found in Table 1 of [58]. In Eq. (5) the emitted GW energy is proportional to $\mathcal{M}_c^{5/3}$, and thus the contributions of light PBH binaries to GWs are negligible.

Combining (4) and (5) yields the GW spectrum from a single PBH stellar bubble and detectable mass parameters

region in the middle and right panels of Fig. 2, respectively. In the middle panel of Fig. 2, with the same total mass, the larger peak mass of PBH mass distribution in the PBH stellar bubble, the more GWs are emitted at the same frequency. Bubbles with peak mass around 10^{15} g emit weak GWs that are difficult to be probed within $(10^{-9}, 10^2)$ Hz. The difficulty of detecting PBH stellar bubble with peak mass around 10^{15} g is also shown in the right panel of Fig. 2, where the total bubble mass should be larger than 10^{53} g with a peak mass less than 10^{23} g at 0.1 Hz for $f_{\text{PBH}} = 10^3$ and $z = 0.01$.

While PBH stellar bubbles with strong Hawking radiation can hardly be probed by the current GW surveys, they may be detectable in some ultra-high frequency GW experiments. Note that the peak energy density in GW spectrum with different peak mass is similar. In Eq. (5), the peak energy radiation occurs at $f_r = f_2$, which is $f_r dE_{\text{GW}}/df_r = (\pi G)^{2/3} (f_2 M)^{5/3} \eta / f_1 = M \eta (a_2 \eta^2 + b_2 \eta + c_2)^{5/3} / (a_1 \eta^2 + b_1 \eta + c_1)$. Comoving merger rate of binaries scales as $R \sim M^{-32/37}$, see [24, 54, 59] for details. Thus, the total radiation power in binaries' rest frame is $R f_r dE_{\text{GW}}/df_r \sim M^{5/37} \eta (a_2 \eta^2 + b_2 \eta + c_2)^{5/3} / (a_1 \eta^2 + b_1 \eta + c_1)$, which depends on symmetric mass ratio η and weakly depends on M . Due to the M_{pk} independence in η distribution, the peak energy density in GW spectrum is weakly dependent on the peak mass in PBH mass distribution. This provides the possibility of detecting GW signals of strong Hawking radiation PBH stellar bubble in ultra-high frequency range.

Concluding remarks – To conclude, we propose the hypothetical possibility of stellar bubbles, which are star-like objects in the sky with exotic features. We focus on a specific class of exotic stellar bubbles filled by lognormal distributed PBHs and analyze their signatures through both the EM and GW observational windows. For the

EM channel, a bubble dominated by light PBHs can yield detectable gamma-ray spectra via Hawking radiation. The peak mass $M_{\text{pk}} \sim 10^{15}$ g and bubble mass $M_{\text{bub}} \sim 10^{32}$ g can be related to the 10 – 100 GeV detection band of Fermi LAT (Fig. 1). Impressively, this scenario can make a decent fit to the ultrahigh-energy gamma-ray events discovered by LHAASO and hence hint to the existence of PBH stellar bubbles with the present peak mass $\tilde{M}_p \sim 10^{10}$ g (the left panel of Fig. 2). For the GWs channel, we find that massive PBH binaries with $M_{\text{pk}} \sim 10^{34} - 10^{38}$ g and $M_{\text{bub}} \sim 10^{45} - 10^{48}$ g can produce detectable GWs within the frequency band of LISA and BBO (the middle panel of Fig. 2).

We comment that, although EM and GW signals from PBH bubbles can hardly be overlapped in the parameter space, these two channels are complementary for light and heavy bubbles. The search for light PBH bubbles can be promising by observing a number of gamma-ray sources whose spectra follow Hawking spectra and their fluxes along the line-of-sight fitting to the light curves of PBH bubbles as displayed in Fig. 1. For heavy bubbles, they can be more accessible by the GW astronomy. These combined limits can further impose the constraint upon the mass function of the PBHs, and thus can shed light on the PBHs formation in the Universe. Accordingly, if such PBH stellar bubbles were observed, it can serve as a novel window to probe the very early Universe.

Additionally, cosmic neutrinos and ultra-high frequency GWs could also be generated from these exotic stellar bubbles. The IceCube Neutrino Observatory has already confirmed the high-energy cosmic neutrinos as the key messengers to reveal an unobstructed view of the Universe at wavelengths where it is opaque to EM signals [60]. On the other hand, the PBH bubbles may leave significant GWs of extremely high frequencies, which urges the development of GW technology in ultra-high frequency bands. We end by mentioning that, while we have discussed astrophysical phenomena of exotic stellar bubbles filled by PBHs, there exist other types of bubbles that produce observable signals, such as collision of cosmic strings [61] and domain walls [62] in the bubbles, matter-antimatter annihilation at their boundaries [63], and so on. These exotic stellar bubbles from the primordial Universe can unveil rich physics hidden in the light of stars, which deserve to be explored in the future.

Acknowledgments – We are grateful to Xiaojun Bi, Ruoyu Liu and Ruizhi Yang for valuable discussions. YFC and CC are supported in part by the NSFC (Nos. 11653002, 11961131007, 11722327, 11421303), by the National Youth Talents Program of China, by the Fundamental Research Funds for Central Universities, by the CSC Innovation Talent Funds, and by the USTC Fellowship for International Cooperation. QD and YW are supported in part by the CRF grant C6017-20GF by the RGC of Hong Kong SAR, and the NSFC EYS (Hong Kong and Macau) Grant No. 12022516. We acknowledge the use of

the clusters *LINDA* and *JUDY* of the particle cosmology group at USTC and computing facilities at HKUST.

SUPPLEMENTARY MATERIAL

Hawking radiation and intrinsic luminosity – In this part, we briefly review the Hawking radiation and intrinsic luminosity of an individual PBH and refer to [39, 40] for comprehensive studies. It was found in [25, 26] that a black hole could emit particles similar to the black-body radiation, with energies in the range $(E, E + dE)$ at a rate

$$\frac{d^2N}{dt dE} = \frac{1}{2\pi} \frac{\Gamma_s(E, M)}{e^{8\pi GME} - (-1)^{2s}}, \quad (6)$$

per particle degree of freedom (e.g. spin, electric charge, flavor and color). Here M is the mass of the black hole, s is the particle spin. In contrast to the astrophysical black holes, PBHs collapsing from the overlarge primordial density perturbations could be small enough for Hawking radiation to be significant. The high-energy particles radiated from PBHs could influence various physical processes in the early Universe. Thus, one can impose evaporation constraints on PBH initial or current abundance via relevant observations, such as Big Bang Nucleosynthesis, CMB and gamma-ray observations. (The detailed discussions can see Refs. [39, 64] and the references therein). According to the radiation rate (6), the black hole temperature can be defined as

$$T_{\text{BH}} = \frac{1}{8\pi GM} \simeq 1.06 \times M_{10}^{-1} \text{ TeV}, \quad (7)$$

where M_{10} is related to the black hole mass $M \equiv M_{10} \times 10^{10}$ g. And $\Gamma_s(E, M)$ is the dimensionless absorption coefficient which accounts for the probability that the particle would be absorbed if it were incident in this state on the black hole. The functional expressions of $\Gamma_s(E, M)$ for massless and massive particles can be found in Refs. [65–67]. Hawking temperature (7) tells us that a smaller black hole is much hotter than a larger black hole, and the emission is also stronger. Note that we adopt the assumption that a black hole has no charge or angular momentum, which is reasonable since charge and angular momentum would also be lost through quantum emission on a shorter time scale than the mass loss time scale [68, 69]; extension to the charged and rotational black holes is straightforward [65–67]. Since a black hole continuously emits particles, its mass decreases while the temperature goes up. The approximate formula for the mass loss rate can be written as [39, 68]

$$\frac{dM_{10}}{dt} \simeq -5.34 \times 10^{-5} \phi(M) M_{10}^{-2} \text{ s}^{-1}, \quad (8)$$

where $\phi(M)$ measures the number of emitted particle species and is normalized to unity for the black holes

with $M \gg 10^{17}$ g, emitting only massless photons, three generations of neutrinos and graviton. The relativistic contributions to $\phi(M)$ per degree of particle freedom are $\phi_{s=0} = 0.267$, $\phi_{s=1} = 0.060$, $\phi_{s=3/2} = 0.020$, $\phi_{s=2} = 0.007$, $\phi_{s=1/2} = 0.147$ (neutral), $\phi_{s=1/2} = 0.142$ (charge $\pm e$) [68]. Integrating the mass loss rate (8) over time then gives the lifetime of a black hole

$$\tau \sim 407 \left(\frac{\phi(M)}{15.35} \right)^{-1} M_{10}^3 \text{ s}. \quad (9)$$

If we sum up the contributions from all the particles in the Standard Model up to 1 TeV, corresponding to $M_{10} \sim 1$, this gives $\phi(M) = 15.35$. The mass of a PBH evaporating at τ after Big Bang is given by [39]

$$M \simeq 1.35 \times 10^9 \left(\frac{\phi(M)}{15.35} \right)^{1/3} \left(\frac{\tau}{1\text{s}} \right)^{1/3} \text{ g}. \quad (10)$$

Thus, the mass of a PBH evaporating at present is roughly $M_* \simeq 5.1 \times 10^{14}$ g (corresponding to $T_{\text{BH}} = 21\text{MeV}$).

Here, we adopt a standard emission picture that a black hole emits only those particles which appear elementary on the scale of the radiated energy (or equivalently the black hole size) [68]. The emitted particles could form composite particles after emission. A black hole should emit all elementary particles whose rest masses are less than or of the order of T_{BH} . The spectra of the particles emitted through the lifetime of PBHs is calculated from the BlackHawk code [47]. When T_{BH} increases, the black hole initially directly emits only photons (and gravitons), then neutrinos, electrons, muons and eventually direct pions join in the emission as T_{BH} surpasses successive particle rest mass thresholds. Once the black hole temperature exceeds QCD energy scale $\Lambda_{\text{QCD}} = 250 - 300\text{MeV}$, the particles radiated can be regarded as asymptotically free, leading to the emission of quarks and gluons. After their emission, quarks and gluons fragment into further quarks and gluons until they cluster into the observable hadrons including protons and antiprotons, electrons, and positrons. Since there are 12 quark degrees of freedom per flavor and 16 gluon degrees of freedom, one would expect the emission rate (i.e., the value of ϕ) to increase suddenly once the QCD temperature is reached. Thus, Hawking radiation is dominated by the decay of QCD particles when the PBHs masses falls below $M_q \simeq 0.4M_* \simeq 2 \times 10^{14}$ g [39, 68, 69].

As discussed above, particles injected from a PBH have two components: the primary component, which is the direct Hawking emission; the secondary component, which comes from the decay of gauge bosons or heavy leptons and the hadrons produced by fragmentation of primary quarks and gluons [39]. For photons, we have

$$\frac{d\dot{N}}{dE}(E, M) = \frac{d\dot{N}^{\text{pri}}}{dE}(E, M) + \frac{d\dot{N}^{\text{sec}}}{dE}(E, M), \quad (11)$$

with similar expressions to other particles. Fig. 3 plots the instantaneous emission rate of photons per

physical cm^3 for PBHs with various horizon masses $10^{15}, 10^{16}, 10^{17}, 10^{20}$ g, and the corresponding energy fraction is set to $f_{\text{PBH}} = 1$. As we expect, the primary photons instantaneous spectrum dominates the high-tail of radiated spectra for the heavy PBHs (i.e., $M > 10^{15}$). This figure is similar to the Fig. 1 in Ref. [39] which shows the instantaneous emission rate of photons for four typical black hole masses.

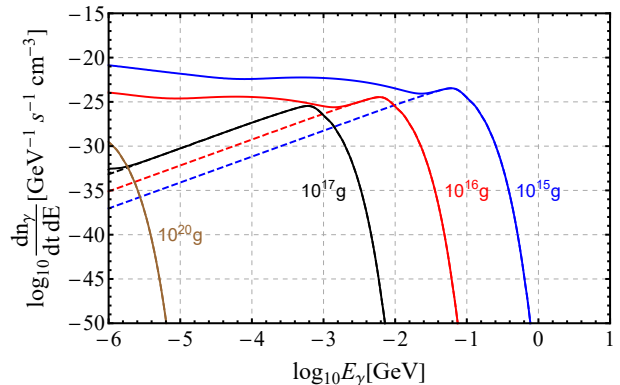


FIG. 3. Instantaneous emission rate of photons per physical cm^3 from PBHs with various horizon masses: $10^{15}, 10^{16}, 10^{17}, 10^{20}$ g, and the corresponding current energy fraction is set to $f_{\text{PBH}} = 1$. The dashed and the solid ones represent the instantaneous primary and total (primary + secondary) emission rates, respectively. We used the open source code BlackHawk [47] to calculate the above photon radiated spectra.

The intrinsic luminosity of Hawking radiation from a PBH bubble is given by

$$L(E, t) = E \frac{d^2 n_\gamma}{dt dE} V dE \simeq E^2 \frac{d^2 n_\gamma}{dt dE} V \quad (12)$$

with dimensions GeV s^{-1} . Note that we used the approximation of the energy interval in the logarithmic scale $dE \simeq E$. Here, E is the emitted photon energy from the PBH bubble. The nearly time-independent behavior of $d^2 n_\gamma / dt dE$ during early times, as shown in Fig. 1, is due to the fact that the major contribution to the mass integral in Eq. (1) is made by the low-mass range above the low bound M_{min} . At the early time, the low-mass range barely changes, which leads to the time-independent instantaneous emission rates $d^2 n_\gamma / dt dE$ in Fig. 1. As the PBHs evaporate, the low bound M_{min} would go up, successively reaching the final evaporation stage of low-mass PBHs, the emission rates thus bump up at a later time. Finally, the emission rate would fade out on account of the evaporation of the low-mass range.

Formation and merger rate of PBH binaries – In this part, we briefly review the formation of PBH binaries and its merger rate. For more details, we would like to refer to [53, 54].

The PBH binary forms when two neighboring black holes are close enough and decouple from the Hubble flow.

Given the equation of motion of two-point masses M at rest with initial separation x , the proper separation r along the axis of motion evolves as

$$\ddot{r} - (\dot{H} + H^2)r + \frac{2M}{r^2} \frac{r}{|r|} = 0, \quad (13)$$

where dots represent the differentiation with respect to proper time. In order to describe the early-Universe evolution, we use $s \equiv a/a_{\text{eq}}$ the scale factor normalized to unity at matter-radiation equality to express the Hubble parameter as $H(s) = (8\pi\rho_{\text{eq}}/3)^{1/2}h(s)$, where h is defined as $h(s) \equiv \sqrt{s^{-3} + s^{-4}}$ and ρ_{eq} is the matter density at equality. Then, we can rewrite Eq. (13) by introducing $\chi \equiv r/x$ as

$$\chi'' + \frac{sh' + h}{s^2h} (s\chi' - \chi) + \frac{1}{\lambda} \frac{1}{(sh)^2} \frac{1}{\chi^2} \frac{\chi}{|\chi|} = 0, \quad (14)$$

where primes denote differentiation with respect to s . Here, the dimensionless parameter λ is defined as $\lambda \equiv 4\pi\rho_{\text{eq}}x^3/3M$. The initial condition is given in the condition that the two neighboring black holes follow the Hubble flow $\chi(s) = s$, the initial conditions are

$$\chi(0) = 0, \quad \chi'(0) = 1. \quad (15)$$

Then, the numerical solution in [53] shows that the binary effectively decouples from the Hubble flow at $s \approx \lambda/3$. The corresponding redshift is

$$z = \frac{3(1 + z_{\text{eq}})}{\lambda} - 1. \quad (16)$$

In order to get the merger rate of PBH binaries with mass distribution $P(m)$ at cosmic time t , we follow [54] and define the binned mass distribution $P(m)$ and mass interval Δ , which follows

$$\sum_{m_{\text{min}}}^{m_{\text{max}}} P(m)\Delta = 1. \quad (17)$$

The average distance between two nearby black holes is

$$\langle x_{ij} \rangle = (\bar{x}_i^{-3} + \bar{x}_j^{-3})^{-1/3} = \mu_{ij}^{1/3} \bar{x}_{ij}, \quad (18)$$

where, μ_{ij} and \bar{x}_{ij} are defined as

$$\begin{aligned} \mu_{ij} &= \frac{2m_i m_j f_b}{m_b f (P(m_j)m_i + P(m_i)m_j)}, \\ \bar{x}_{ij}^3 &= \frac{3}{8\pi} \frac{m_b}{\rho_{\text{eq}} f_b \Delta}, \end{aligned} \quad (19)$$

where, $f_b = f(P(m_i) + P(m_j))$ and $m_b = m_i + m_j$. Here, f is the fraction of PBH energy density in matter. The relation of f and f_{PBH} is $f \approx 0.85f_{\text{PBH}}$. After the binary forms, GWs are emitted from the PBH binary. The coalescence time of the PBH binary is given in [70] by

$$t = \frac{3}{85} \frac{a^4}{G^3 m_1 m_2 M} j^7. \quad (20)$$

From Eq. (20), the merger rate of PBH binaries can be obtained from the initial semi-major axis a distribution and the initial dimensionless angular momentum j distribution. The initial semi-major axis a after the binary formation is numerically given in [53],

$$a \approx 0.1\lambda x = \frac{0.1\bar{x}_{ij}}{f_b \Delta} X^{4/3}, \quad (21)$$

where, $X \equiv x^3/\bar{x}_{ij}^3$. Therefore, the initial semi-major axis distribution is determined by the separation x distribution, we follow [53, 54] that assuming PBHs follow a random distribution, the probability distribution of the separation x is

$$\frac{dP}{dX} = \mu_{ij}^{-1} e^{-X \frac{4\pi}{3} \bar{x}_{ij}^3 n_T}, \quad (22)$$

where $n_T \equiv f_{\text{PBH}}\rho_{\text{DM}}(1 + z_{\text{eq}})^3 \int_0^\infty \frac{P(m)}{m} dm$. Considering fixed X , the dimensionless angular momentum j can be given by Eq. (20) and Eq. (21),

$$j(t; X) = \left(\frac{3}{85} \frac{G^3 m_1 m_2 M (f_b \Delta)^4}{(0.1\bar{x}_{ij})^4 X^{16/3}} t \right)^{1/7}. \quad (23)$$

The differential probability distribution of (X, t) is given by

$$\begin{aligned} \frac{d^2 P}{dX dt} &= \frac{dP}{dX} \left(\frac{\partial j}{\partial t} \frac{dP}{dj} \Big|_X \right)_{j(t; X)} \\ &= \frac{\mu_{ij}^{-1}}{7t} e^{-X \frac{4\pi}{3} \bar{x}_{ij}^3 n_T} \mathcal{P}(j/j_X), \end{aligned} \quad (24)$$

where $j_X = 0.5fX/f_b\Delta$, $\mathcal{P}(j/j_X) = (j/j_X)^2/(1 + j^2/j_X^2)^{3/2}$. Integrating Eq. (24) gives the merger time probability distribution

$$\frac{dP}{dt} = \frac{\mu_{ij}^{-1}}{7t} \int dX e^{-X \frac{4\pi}{3} \bar{x}_{ij}^3 n_T} \mathcal{P}(j/j_X). \quad (25)$$

Then, the comoving merger rate R_{ij} for binary system at time t is

$$R_{ij}(t) = \rho_{\text{PBH}} \min \left(\frac{P(m_i)}{m_i}, \frac{P(m_j)}{m_j} \right) \Delta \frac{dP}{dt}. \quad (26)$$

The merger rate for the whole PBH distribution can be obtained by summarizing all the binaries system,

$$R(t) = \sum_{\substack{0 < m_i < m_j \\ 0 < m_j < \infty}} \rho_{\text{PBH}} \min \left(\frac{P(m_i)}{m_i}, \frac{P(m_j)}{m_j} \right) \Delta \frac{dP}{dt}. \quad (27)$$

GW spectrum – The GW energy flux from a distant source can be expressed as the following form [71],

$$S(t) = \frac{L_{\text{GW}}(t)}{4\pi d_L^2}, \quad (28)$$

where $L_{\text{GW}}(t)$ is the GW luminosity measured in the PBH rest frame. Then, integrating $S(t)$ over the PBH binary evolution gives the observed redshifted GW energy, which is

$$\begin{aligned} \int_{-\infty}^{\infty} S(t)dt &= \frac{1+z}{4\pi d_L^2} \int_{-\infty}^{\infty} L_{\text{GW}}(t_r)dt_r \\ &= \frac{1+z}{4\pi d_L^2} \int_0^{\infty} \frac{dE_{\text{GW}}}{df_r} df_r. \end{aligned} \quad (29)$$

Here the relation of time measured in the rest frame of source and observed frame is $t_r = t/(1+z)$. The observed energy density can be expressed as

$$\begin{aligned} \rho_{\text{GW}} &= \int_0^{\infty} \Omega_{\text{GW}}(f) \rho_c \frac{df}{f} \\ &= \int_{z_{\min}}^{z_{\max}} \frac{1+z}{4\pi d_L^2} \left(\int_0^{\infty} f_r \frac{dE_{\text{GW}}}{df_r} \frac{df}{f} \right) \frac{dN}{dt dz} dz. \end{aligned} \quad (30)$$

Here, $dN/dtdz$ is the number of merger events which occur in dt between redshift z and $z+dz$. Therefore, Ω_{GW} can be written as

$$\Omega_{\text{GW}}(f) = \frac{1}{\rho_c} \frac{1}{4\pi d_L^2} f_r \frac{dE_{\text{GW}}}{df_r} \int_{z_{\min}}^{z_{\max}} (1+z) \frac{dN}{dt dz} dz. \quad (31)$$

Compare with the cosmic distance, the comoving size of PBH stellar bubble is relatively small, so that $\Delta z = z_{\max} - z_{\min}$ is tiny. Eq. (31) can be written as

$$\begin{aligned} \Omega_{\text{GW}}(f) &= \frac{1}{\rho_c} \frac{1}{4\pi d_L^2} f_r \frac{dE_{\text{GW}}}{df_r} \frac{dN}{dt} \\ &= \frac{1}{\rho_c} \frac{1}{4\pi d_L^2} f_r \frac{dE_{\text{GW}}}{df_r} R. \end{aligned} \quad (32)$$

From the Eq. (32), we can get the GW spectrum from the single PBH stellar bubble in Fig. 4.

In Fig. 4, the GW energy density from the PBH stellar bubble with small peak mass is weak in detection. However, the peak energy density of PBH stellar bubble weakly depends on the peak mass. In Eq. (5), the peak energy radiation occurs at $f_r = f_2$, so

$$\begin{aligned} f_r \frac{dE_{\text{GW}}}{df_r} &= (\pi G)^{2/3} \eta \frac{(f_2 M)^{5/3}}{f_1} \\ &= M \eta \frac{(a_2 \eta^2 + b_2 \eta + c_2)^{5/3}}{a_1 \eta^2 + b_1 \eta + c_1}. \end{aligned} \quad (33)$$

In Eq. (27), $R \sim M^{-32/37}$, see [24, 54, 59] for details. As the result, the peak radiation power in the rest frame of PBH stellar bubble is

$$\begin{aligned} R f_r \frac{dE_{\text{GW}}}{df_r} &\sim M^{5/37} \eta \frac{(a_2 \eta^2 + b_2 \eta + c_2)^{5/3}}{a_1 \eta^2 + b_1 \eta + c_1} \\ &\sim M_{\text{pk}}^{5/37} (\gamma_1 + \gamma_2)^{5/37} \eta \frac{(a_2 \eta^2 + b_2 \eta + c_2)^{5/3}}{a_1 \eta^2 + b_1 \eta + c_1}. \end{aligned} \quad (34)$$

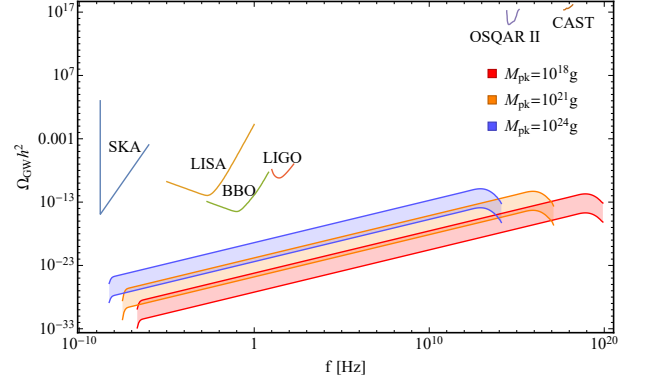


FIG. 4. The GW spectrum of a single PBH stellar bubble. The $f_{\text{PBH}} = 1$ in PBH stellar bubble and redshift of bubble is set as $z = 0.01$. The extended mass distribution of PBH is log-normal distribution with $\sigma = 1$ and $M_{\text{pk}} = 10^{18}\text{g}, 10^{21}\text{g}, 10^{24}\text{g}$ for red, orange, blue shadow region respectively. The lower solid line and upper solid line denote the total PBH mass in bubble which is set as 10^{45}g and the 10^{48}g respectively. Sensitivity curve below 1000Hz from SKA, LISA, BBO and LIGO are plotted. Sensitivity curve in ultra-high frequency range from OSQAR [72] and CAST [73] are also plotted.

Here, we define mass ratio $\gamma_i \equiv m_i/M_{\text{pk}}$. The γ and η can be shown that they are independent on the M_{pk} in lognormal distribution as following,

$$\begin{aligned} \psi_{\text{LN}}(M)dM &= \frac{f_{\text{PBH}}}{\sqrt{2\pi\sigma M}} \exp\left[-\frac{\ln^2(M/M_{\text{pk}})}{2\sigma^2}\right] dM \\ &= \frac{f_{\text{PBH}}}{\sqrt{2\pi\sigma\gamma M_{\text{pk}}}} \exp\left[-\frac{\ln^2(\gamma)}{2\sigma^2}\right] M_{\text{pk}} d\gamma. \end{aligned} \quad (35)$$

Therefore, the γ distribution is

$$\psi_{\text{LN}}(\gamma)d\gamma = \frac{f_{\text{PBH}}}{\sqrt{2\pi\sigma\gamma}} \exp\left[-\frac{\ln^2(\gamma)}{2\sigma^2}\right] d\gamma, \quad (36)$$

which is independent with M_{pk} . η can be expressed as

$$\eta = \frac{m_1 m_2}{(m_1 + m_2)^2} = \frac{\gamma_1 \gamma_2}{(\gamma_1 + \gamma_2)^2}, \quad (37)$$

which is also independent with M_{pk} . Therefore Eq. (34) shows the peak energy density depends on the $M_{\text{pk}}^{5/37}$, which weakly depends on the peak mass in PBH distribution.

* yifucai@ustc.edu.cn
† cchao012@mail.ustc.edu.cn
‡ qdingab@connect.ust.hk
§ phyw@ust.hk

[1] S. R. Kelner, Felix A. Aharonian, and V. V. Bugayov. Energy spectra of gamma-rays, electrons and neutrinos

- produced at proton-proton interactions in the very high energy regime. *Phys. Rev. D*, 74:034018, 2006. [Erratum: *Phys.Rev.D* 79, 039901 (2009)].
- [2] Andrew W. Strong, Igor V. Moskalenko, and Vladimir S. Ptuskin. Cosmic-ray propagation and interactions in the Galaxy. *Ann. Rev. Nucl. Part. Sci.*, 57:285–327, 2007.
- [3] E. G. Berezhko and L. T. Ksenofontov. Composition of cosmic rays accelerated in supernova remnants. *J. Exp. Theor. Phys.*, 89:391–403, 1999.
- [4] K. Kobayakawa, Y. Sato, and T. Samura. Acceleration of particles by oblique shocks and cosmic ray spectra around the knee region. *Phys. Rev. D*, 66:083004, 2002.
- [5] B. P. Abbott et al. Multi-messenger Observations of a Binary Neutron Star Merger. *Astrophys. J. Lett.*, 848(2):L12, 2017.
- [6] B. P. Abbott et al. Tests of general relativity with GW150914. *Phys. Rev. Lett.*, 116(22):221101, 2016. [Erratum: *Phys.Rev.Lett.* 121, 129902 (2018)].
- [7] Péter Mészáros, Derek B. Fox, Chad Hanna, and Kōhta Murase. Multi-Messenger Astrophysics. *Nature Rev. Phys.*, 1:585–599, 2019.
- [8] D. D. Ivanenko and D. F. Kurdgelaidze. Hypothesis concerning quark stars. *Astrophysics*, 1:251–252, 1965.
- [9] David J. Kaup. Klein-Gordon Geon. *Phys. Rev.*, 172:1331–1342, 1968.
- [10] Douglas Spolyar, Katherine Freese, and Paolo Gondolo. Dark matter and the first stars: a new phase of stellar evolution. *Phys. Rev. Lett.*, 100:051101, 2008.
- [11] Simon Dupourqué, Luigi Tibaldo, and Peter Von Ballmoos. Constraints on the antistar fraction in the Solar System neighborhood from the 10-year Fermi Large Area Telescope gamma-ray source catalog. *Phys. Rev. D*, 103(8):083016, 2021.
- [12] Sidney R. Coleman and Frank De Luccia. Gravitational Effects on and of Vacuum Decay. *Phys. Rev.*, D21:3305, 1980.
- [13] Zihan Zhou, Jun Yan, Andrea Addazi, Yi-Fu Cai, Antonino Marciano, and Roman Pasechnik. Probing new physics with multi-vacua quantum tunnelings beyond standard model through gravitational waves. *Phys. Lett. B*, 812:136026, 2021.
- [14] Miao Li and Yi Wang. Multi-Stream Inflation. *JCAP*, 07:033, 2009.
- [15] Andrew G. Cohen, A. De Rujula, and S. L. Glashow. A Matter - antimatter universe? *Astrophys. J.*, 495:539–549, 1998.
- [16] Zhen Cao et al. Ultrahigh-energy photons up to 1.4 petaelectronvolts from 12 γ -ray galactic sources. *Nature*, May 2021.
- [17] Y. B. Zel’dovich and I. D. Novikov. The Hypothesis of Cores Retarded during Expansion and the Hot Cosmological Model. *Sov. Astron.*, 10:602, 1966.
- [18] Stephen Hawking. Gravitationally collapsed objects of very low mass. *Mon. Not. Roy. Astron. Soc.*, 152:75, 1971.
- [19] Bernard J. Carr and S. W. Hawking. Black holes in the early Universe. *Mon. Not. Roy. Astron. Soc.*, 168:399–415, 1974.
- [20] Maxim Yu. Khlopov. Primordial Black Holes. *Res. Astron. Astrophys.*, 10:495–528, 2010.
- [21] Misao Sasaki, Teruaki Suyama, Takahiro Tanaka, and Shuichiro Yokoyama. Primordial black holes—perspectives in gravitational wave astronomy. *Class. Quant. Grav.*, 35(6):063001, 2018.
- [22] Bernard Carr, Florian Kuhnel, and Marit Sandstad. Primordial Black Holes as Dark Matter. *Phys. Rev.*, D94(8):083504, 2016.
- [23] Simeon Bird, Ilias Cholis, Julian B. Muñoz, Yacine Ali-Haïmoud, Marc Kamionkowski, Ely D. Kovetz, Alvise Raccanelli, and Adam G. Riess. Did LIGO detect dark matter? *Phys. Rev. Lett.*, 116(20):201301, 2016.
- [24] Misao Sasaki, Teruaki Suyama, Takahiro Tanaka, and Shuichiro Yokoyama. Primordial Black Hole Scenario for the Gravitational-Wave Event GW150914. *Phys. Rev. Lett.*, 117(6):061101, 2016. [Erratum: *Phys.Rev.Lett.* 121, 059901 (2018)].
- [25] S. W. Hawking. Black hole explosions. *Nature*, 248:30–31, 1974.
- [26] S. W. Hawking. Particle Creation by Black Holes. *Commun. Math. Phys.*, 43:199–220, 1975. [Erratum: *Commun.Math.Phys.* 46, 206 (1976)].
- [27] Jane H. MacGibbon and Bernard J. Carr. Cosmic rays from primordial black holes. *Astrophys. J.*, 371:447–469, 1991.
- [28] Yi-Fu Cai, Xi Tong, Dong-Gang Wang, and Sheng-Feng Yan. Primordial Black Holes from Sound Speed Resonance during Inflation. *Phys. Rev. Lett.*, 121(8):081306, 2018.
- [29] Chao Chen and Yi-Fu Cai. Primordial black holes from sound speed resonance in the inflaton-curvaton mixed scenario. *JCAP*, 1910(10):068, 2019.
- [30] Bernard Carr and Florian Kuhnel. Primordial black holes with multimodal mass spectra. *Phys. Rev.*, D99(10):103535, 2019.
- [31] Zihan Zhou, Jie Jiang, Yi-Fu Cai, Misao Sasaki, and Shi Pi. Primordial black holes and gravitational waves from resonant amplification during inflation. *Phys. Rev. D*, 102(10):103527, 2020.
- [32] Alexandre Dolgov and Joseph Silk. Baryon isocurvature fluctuations at small scales and baryonic dark matter. *Phys. Rev. D*, 47:4244–4255, 1993.
- [33] B. J. Carr, Kazunori Kohri, Yuuiti Sendouda, and Jun’ichi Yokoyama. Constraints on primordial black holes from the Galactic gamma-ray background. *Phys. Rev. D*, 94(4):044029, 2016.
- [34] Don N. Page and S. W. Hawking. Gamma rays from primordial black holes. *Astrophys. J.*, 206:1–7, 1976.
- [35] G Weidenspointner, M Varendorff, SC Kappadath, K Bennett, H Bloemen, R Diehl, W Hermsen, GG Lichti, J Ryan, and V Schönfelder. The cosmic diffuse gamma-ray background measured with comptel. In *AIP Conference Proceedings*, volume 510, pages 467–470. American Institute of Physics, 2000.
- [36] A. W. Strong, I. V. Moskalenko, and O. Reimer. A new determination of the extragalactic diffuse gamma-ray background from egret data. *Astrophys. J.*, 613:956–961, 2004.
- [37] W. B. Atwood et al. The Large Area Telescope on the Fermi Gamma-ray Space Telescope Mission. *Astrophys. J.*, 697:1071–1102, 2009.
- [38] Bernard J. Carr and J. H. MacGibbon. Cosmic rays from primordial black holes and constraints on the early universe. *Phys. Rept.*, 307:141–154, 1998.
- [39] B. J. Carr, Kazunori Kohri, Yuuiti Sendouda, and Jun’ichi Yokoyama. New cosmological constraints on primordial black holes. *Phys. Rev.*, D81:104019, 2010.
- [40] T. N. Ukwatta, D. R. Stump, J. T. Linnemann, J. H. MacGibbon, S. S. Marinelli, T. Yapici, and K. Tollefson. Primordial Black Holes: Observational Characteristics of The Final Evaporation. *Astropart. Phys.*, 80:90–114,

- 2016.
- [41] Sunghoon Jung and TaeHun Kim. Gamma-ray burst lensing parallax: Closing the primordial black hole dark matter mass window. *Phys. Rev. Res.*, 2(1):013113, 2020.
- [42] Scott Dodelson. *Modern Cosmology*. Academic Press, Amsterdam, 2003.
- [43] V. Mukhanov. *Physical Foundations of Cosmology*. Cambridge University Press, Oxford, 2005.
- [44] A. Albert et al. Evidence that Ultra-high-energy Gamma Rays Are a Universal Feature near Powerful Pulsars. *Astrophys. J. Lett.*, 911(2):L27, 2021.
- [45] Roland Kothés, Bulent Uyaniker, and Serge Pineault. The snr g106.3+2.7 and its pulsar wind nebula: relics of triggered star formation in a complex environment. *Astrophys. J.*, 560:236, 2001.
- [46] Liang Chen, Zheng Xiong, Cong Li, SongZhan Chen, and HuiHai He. Strong constraints on Lorentz violation using new γ -ray observations around PeV. 5 2021.
- [47] Alexandre Arbey and J er emy Auffinger. BlackHawk: A public code for calculating the Hawking evaporation spectra of any black hole distribution. *Eur. Phys. J. C*, 79(8):693, 2019.
- [48] P. E. Dewdney, P. J. Hall, R. T. Schilizzi, and T. J. L. W. Lazio. The Square Kilometre Array. *IEEE Proceedings*, 97(8):1482–1496, August 2009.
- [49] P Bender, A Brillet, I Ciufolini, AM Cruise, C Cutler, K Danzmann, F Fidicaro, WM Folkner, J Hough, P McNamara, et al. Lisa pre-phase a report. *Max-Planck Institut f ur Quantenoptik*, 1998.
- [50] Jeff Crowder and Neil J. Cornish. Beyond LISA: Exploring future gravitational wave missions. *Phys. Rev. D*, 72:083005, 2005.
- [51] B. P. Abbott et al. LIGO: The Laser interferometer gravitational-wave observatory. *Rept. Prog. Phys.*, 72:076901, 2009.
- [52] N. Aghanim et al. Planck 2018 results. VI. Cosmological parameters. *Astron. Astrophys.*, 641:A6, 2020.
- [53] Yacine Ali-Ha imoud, Ely D. Kovetz, and Marc Kamionkowski. Merger rate of primordial black-hole binaries. *Phys. Rev. D*, 96(12):123523, 2017.
- [54] Zu-Cheng Chen and Qing-Guo Huang. Merger Rate Distribution of Primordial-Black-Hole Binaries. *Astrophys. J.*, 864(1):61, 2018.
- [55] C. Cutler, Eric Poisson, G. J. Sussman, and L. S. Finn. Gravitational radiation from a particle in circular orbit around a black hole. 2: Numerical results for the nonrotating case. *Phys. Rev. D*, 47:1511–1518, 1993.
- [56] David F. Chernoff and Lee Samuel Finn. Gravitational radiation, inspiraling binaries, and cosmology. *Astrophys. J. Lett.*, 411:L5–L8, 1993.
- [57] Xing-Jiang Zhu, E. Howell, T. Regimbau, D. Blair, and Zong-Hong Zhu. Stochastic Gravitational Wave Background from Coalescing Binary Black Holes. *Astrophys. J.*, 739:86, 2011.
- [58] P. Ajith et al. A Template bank for gravitational waveforms from coalescing binary black holes. I. Non-spinning binaries. *Phys. Rev. D*, 77:104017, 2008. [Erratum: *Phys.Rev.D* 79, 129901 (2009)].
- [59] Qianhang Ding, Tomohiro Nakama, Joseph Silk, and Yi Wang. Detectability of Gravitational Waves from the Coalescence of Massive Primordial Black Holes with Initial Clustering. *Phys. Rev. D*, 100(10):103003, 2019.
- [60] M. G. Aartsen et al. Evidence for High-Energy Extraterrestrial Neutrinos at the IceCube Detector. *Science*, 342:1242856, 2013.
- [61] E. P. S. Shellard. Cosmic String Interactions. *Nucl. Phys. B*, 283:624–656, 1987.
- [62] Yu-ichi Takamizu and Kei-ichi Maeda. Collision of domain walls and reheating of the brane universe. *Phys. Rev. D*, 70:123514, 2004.
- [63] S. I. Blinnikov, A. D. Dolgov, and K. A. Postnov. Antimatter and antistars in the universe and in the Galaxy. *Phys. Rev. D*, 92(2):023516, 2015.
- [64] Bernard Carr, Kazunori Kohri, Yuuiti Sendouda, and Jun’ichi Yokoyama. Constraints on Primordial Black Holes. 2 2020.
- [65] Don N. Page. Particle Emission Rates from a Black Hole: Massless Particles from an Uncharged, Nonrotating Hole. *Phys. Rev. D*, 13:198–206, 1976.
- [66] Don N. Page. Particle Emission Rates from a Black Hole. 2. Massless Particles from a Rotating Hole. *Phys. Rev. D*, 14:3260–3273, 1976.
- [67] Don N. Page. Particle Emission Rates from a Black Hole. 3. Charged Leptons from a Nonrotating Hole. *Phys. Rev. D*, 16:2402–2411, 1977.
- [68] J. H. MacGibbon and B. R. Webber. Quark and gluon jet emission from primordial black holes: The instantaneous spectra. *Phys. Rev. D*, 41:3052–3079, 1990.
- [69] Jane H. MacGibbon. Quark and gluon jet emission from primordial black holes. 2. The Lifetime emission. *Phys. Rev. D*, 44:376–392, 1991.
- [70] P. C. Peters. Gravitational Radiation and the Motion of Two Point Masses. *Phys. Rev.*, 136:B1224–B1232, 1964.
- [71] E. S. Phinney. A Practical theorem on gravitational wave backgrounds. 7 2001.
- [72] P. Pugn at et al. Search for weakly interacting sub-eV particles with the OSQAR laser-based experiment: results and perspectives. *Eur. Phys. J. C*, 74(8):3027, 2014.
- [73] V. Anastassopoulos et al. New CAST Limit on the Axion-Photon Interaction. *Nature Phys.*, 13:584–590, 2017.